Paper to be submitted to the American Nuclear Society, PHYSOR 2000, Pittsburgh, PA,, May 7-11, 2000.

Development of A Coupled Dynamics Code with Transport Theory Capability and Application to Accelerator Driven Systems Transients

J. E. Cahalan
Argonne National Laboratory
Reactor Analysis Division
9700 S. Cass Avenue
Argonne, IL 60439

T. Ama
Osaka University
Department of Nuclear Engineering
2-1, Yamadaoka, Suita
Osaka, Japan

G. Palmiotti, T. A. Taiwo, and W. S. Yang
Argonne National Laboratory
Reactor Analysis Division .
9700 South Cass Avenue
Argonne, IL 60439

DISCLAIMER

DISCLAIMER

Portions of this document may be illegible in electronic image products. Images are produced from the best available original document.

DEVELOPMENT OF A COUPLED DYNAMICS CODE
WITH TRANSPORT THEORY CAPABILITY AND
APPLICATION TO ACCELERATOR-DRIVEN SYSTEMS TRANSIENTS

J. E. Cahalan
Argonne National Laboratory
Reactor Analysis Division
9700 South Cass Avenue
Argonne, Illinois 60439
jecahalan@anl.gov

T. Ama
Osaka University
Department of Nuclear Engineering
2-1, Yamadaoka, Suita
Osaka, Japan
tama@nucl.eng.osaka-u.ac.jp

G. Palmiotti, T. A. Taiwo, and W. S. Yang[*]
Argonne National Laboratory
Reactor Analysis Division
9700 South Cass Avenue
Argonne, Illinois 60439
gpalmiotti@anl.gov ; taiwo@anl.gov ; wyang@ra.anl.gov

[*]Permanent Address:Department of Nuclear Engineering, Chosun University,
P.O. Box 275, Kwangju, 501-600, Korea

ABSTRACT

The VARIANT-K and DIF3D-K nodal spatial kinetics computer codes have been coupled to the SAS4A and SASSYS-1 liquid metal reactor accident and systems analysis codes. SAS4A and SASSYS-1 have been extended with the addition of heavy liquid metal (Pb and Pb-Bi) thermophysical properties, heat transfer correlations, and fluid dynamics correlations. The coupling methodology and heavy liquid metal modeling additions are described. The new computer code suite has been applied to analysis of neutron source and thermal-hydraulics transients in a model of an accelerator-driven minor actinide burner design proposed in an OECD/NEA/NSC benchmark specification. Modeling assumptions and input data generation procedures are described. Results of transient analyses are reported, with emphasis on comparison of P1 and P3 variational nodal transport theory results with nodal diffusion theory results, and on significance of spatial kinetics effects.

1. INTRODUCTION

Recent international interest in using accelerator-driven subcritical systems to fission long-lived, transuranic isotopes produced during irradiation of nuclear power reactor fuel has prompted the evaluation of engineered design features of such concepts[1]. This paper presents the results of a study contributing to this evaluation process, a study focusing on identification of computational methods required for accurate analysis of coupled spatial neutron kinetics and thermal-hydraulics effects in heavy-liquid-metal-cooled (HLMC), fast spectrum, subcritical reactors.

During the study, both a nodal transport theory spatial kinetics code and a nodal diffusion theory spatial kinetics code were coupled to a liquid-metal-coolant reactor analysis computer code system to provide the primary evaluation tools. The newly-coupled codes were applied to analyses of neutron source and coolant hydraulics transients in a prototypic conceptual design. Following descriptions of the spatial kinetics and thermal hydraulics codes, this paper provides a summary description of the accelerator-driven subcritical reactor design, and the methods employed for preparation of cross section and neutron source data. Transient analysis results are presented that characterize the impact of spatial kinetics and higher-order transport effects in coupled neutronics/thermal-hydraulics analyses.

2. COUPLED SPATIAL KINETICS AND THERMAL HYDRAULICS CODES

2.1 VARIANT-K

The VARIANT[2] computer code solves the equilibrium multigroup neutron diffusion and transport equations in two- and three-dimensional Cartesian and hexagonal geometries using variational nodal methods. The transport approximations involve complete spherical harmonic expansions up to order P5. Eigenvalue, adjoint, fixed source, gamma heating, and criticality (concentration) search problems are permitted. Anisotropic scattering is treated, and although primarily designed for fast reactor problems, upscattering options are also included.

The multigroup neutron transport equations are solved using a variational nodal method[3-6] with one mesh cell (node) per hexagonal subassembly and Cartesian geometry node sizes specified by the user. The nodal equations are derived from a functional incorporating nodal balance, and reflective and vacuum boundary conditions through Lagrange multipliers. Expansion of the functional in orthogonal spatial and angular (spherical harmonics) polynomials leads to a set of response matrix equations relating partial current moments to flux and source moments. Flux and source spatial expansions of up to sixth order are allowed. Partial current spatial expansions up to second order are allowed. Angular and scattering expansions up to P5 are allowed. The equations are solved by fission source iteration in conjunction with a coarse mesh rebalance acceleration scheme. The inner iterations are accelerated by a partitioned matrix scheme equivalent to a synthetic diffusion acceleration method.

Variational nodal methods incorporate a number of attractive features. These include a standard hierarchy of space-angle approximation, well behaved small mesh limits, and the absence of both ray effects and artificial diagonal streaming depressions. Dimensionless parts of the response matrices involving integrals in space and angle are pre-computed once and for all using

MATHEMATICA for each geometry option. The results are stored in FORTRAN data statements and used at the time of execution to generate response matrix sets for unique nodes (defined by cross section and dimension data) prior to fission source iteration. VARIANT achieves near Monte Carlo accuracy at a fraction of the cost. VARIANT is implemented as a computational module in the DIF3D[7] code system at Argonne National Laboratory.

The variational nodal method employed in VARIANT was recently extended to solve the time-dependent neutron transport equation by Rineiski[8] and Doriath at Centre d'Etude de Cadarache. In this work, two formulations were implemented, the direct method and the space-time factorization method. In the direct method, the time-dependent problem is simulated with an implicit first-order finite-difference scheme. In the factorization method, the neutron flux is factored into a rapidly-varying amplitude function depending only on time and a slowly-varying shape function depending on space, angle, and time. The factorization formulation[9], when implemented as in the improved quasistatic computational method[10], reduces to point kinetics with the reactivity calculated according to the rigorous formulation, the adiabatic approximation, or in the limit to first order perturbation theory, depending on the frequency of flux shape recalculation. Both the direct and factorization methods reduce the time-dependent problem to a sequence of "fixed source" problems, which may be computed with repeated executions of an existing equilibrium flux solution algorithm. In these flux solutions, the external source and some of the group constants are modified to include time-dependent contributions. The spatial kinetics module constructed by Rineiski and Doriath has been implemented at Argonne National Laboratory in connection with VARIANT to produce the transport theory spatial kinetics capability called VARIANT-K[11].

2.2 DIF3D-K

The DIF3D-K[12-17] computer code solves the multigroup time-dependent neutron diffusion equations (with or without an external neutron source) in two- and three-dimensional hexagonal and Cartesian geometries. All steady-state calculational options of the base time-independent DIF3D[7] are retained.

The time-dependent multigroup neutron diffusion equations are discretized in both space and time. A nodal method[13] employing one radial node per hexagonal subassembly and one or more radial nodes per subassembly in Cartesian geometry is used for spatial discretization. The nodal equations are derived using polynomial approximations to the spatial dependence of the flux within each node. The resulting equations are the time-dependent nodal equations for the neutron flux and precursor concentration moments, and the response matrix equations which relate the flux moments to the surface-averaged partial currents across nodal interfaces. The time-dependent nodal equations are solved with one of two major time discretization schemes: the theta method or the space-time factorization method. The theta method is a variable time integration scheme which permits the resulting difference equations to range from fully explicit to fully implicit. For a given value of the variable parameter theta, the solution of the time-dependent nodal equations reduces to a sequence of "fixed source" problems in which the fixed source term is composed of quantities computed from the solution of the previous time point. In each fixed source problem, the unknown flux moments and interface partial currents are computed using a conventional fission source iteration accelerated by coarse-mesh rebalance and asymptotic source extrapolation. At each fission source iteration, the interface partial currents for each neutron energy group are determined from the response matrix equations with a known

group source term. The factorization method allows the use of the improved quasistatic[10], adiabatic, or conventional point kinetics option for treatment of the time dependence. In the improved quasistatic option, the same algorithm used for the fully implicit theta scheme is employed with large time-step sizes to determine the flux shapes. In the adiabatic option a series of time-independent eigenvalue problems are employed to obtain the flux shapes. In the conventional point kinetics scheme, the initial steady-state shape is used for the duration of the transient problem. In all these factorization options, the flux amplitude is obtained from the solution of the point kinetics equations employing time-dependent kinetics parameters evaluated by the code.

2.3 SAS4A/SASSYS-1

The physical models in the SAS4A and SASSYS-1 computer codes[18,19] are highly detailed mathematical representations of the reactor and coolant loops behavior in transient and accident conditions based on extensive laboratory and test reactor results. The models were originally specialized to liquid sodium cooled fast reactors with oxide or metallic fuel clad with stainless steel.

The SAS4A computer code is designed to perform deterministic analysis of severe accidents in liquid metal cooled reactors (LMRs). Detailed, mechanistic models of steady-state and transient thermal, hydraulic, neutronic, and mechanical phenomena are employed to describe the response of the reactor core and its coolant, fuel elements, and structural members to accident conditions caused by loss of coolant flow, loss of heat rejection, or reactivity insertion. The initiating phase of the accident is modeled, including coolant heating and boiling, fuel cladding failure, and fuel melting and relocation. SAS4A analysis is terminated upon loss of subassembly hexcan integrity. The objective of SAS4A analysis is to quantify severe accident consequences as measured by the generation of energetics sufficient to challenge reactor vessel integrity, leading possibly to public health and safety risk.

The SASSYS-1 computer code is designed to perform deterministic analysis of design basis and beyond-design basis accidents in liquid metal cooled reactor (LMR) plants. Detailed, mechanistic models of steady-state and transient thermal, hydraulic, neutronic, and mechanical phenomena are employed to describe the response of the reactor core, the reactor primary and secondary coolant loops, the reactor control and protection systems, and the balance-of-plant to accidents caused by loss of coolant flow, loss of heat rejection, or reactivity insertion. The consequences of single and double-fault accidents are modeled, including fuel and coolant heating, fuel and cladding mechanical behavior, core reactivity feedbacks, coolant loops performance including natural circulation, and decay heat removal. SASSYS-1 analysis is terminated upon demonstration of reactor and plant shutdown to permanently coolable conditions, or upon violation of design basis margins. The objective of SASSYS-1 analysis is to quantify accident consequences as measured by the transient behavior of system performance parameters, such as fuel and cladding temperatures, reactivity, and cladding strain.

In space, each SAS4A/SASSYS-1 channel models a fuel pin and its associated coolant. A channel represents one or more fuel pins in a single or multiple pin model of a subassembly. In a single pin model, a channel represents all of the pins in a subassembly, and possibly all the pins in a group of subassemblies. In a multiple pin model, many channels are employed to represent a subassembly. In either case, many channels are usually employed for a whole-core

representation. Heat transfer in each pin is modeled with a two-dimensional (r/z) heat conduction equation. Single and two-phase coolant thermal-hydraulics are simulated with a unique, one-dimensional (axial) multiple-bubble liquid metal boiling model. The transient fuel and cladding mechanical behavior model, integrated with fission product production, release, and transport models, provides prediction of fuel element dimensional changes, margins to cladding failure, and cladding failure time and location. In SAS4A, fuel and cladding melting and subsequent relocation are described with multiple-component fluid dynamics models, with material motions driven by gravity and pressures from coolant vaporization, fission gas liberation, and fuel and cladding vaporization. Thermal-hydraulic models of the reactor and intermediate coolant loops analyze heat removal from both forced and natural circulation, with transient performance of loop components including pumps, heat exchangers, valves, and plena. The balance-of-plant thermal-hydraulic model performs transient simulation of the feedwater/steam system. Both the coolant loop model and the balance-of-plant model are integrated with the plant protection and control system model, which is used to simulate the performance of reactor scram systems, as well as controllers on pumps, valves, and decay heat removal systems. Reactivity feedbacks from fuel heating (axial expansion and Doppler), coolant heating and boiling, and fuel and cladding relocation are tracked. Reactivity effects from reactor structural temperature changes yielding radial core expansion are modeled. Numerical solution methods used in the code modules range from semi-implicit to explicit. The coupling of all thermal/hydraulics modules in time is semi-explicit within a multiple-level time step framework.

2.4 SPATIAL KINETICS COUPLING WITH THERMAL HYDRAULICS

The coupling of VARIANT-K and DIF3D-K with SAS4A/SASSYS-1 was accomplished with the construction of an interface module that performs data communications between the thermal/hydraulic module (SAS4A/SASSYS-1) and the spatial kinetics module (VARIANT-K or DIF3D-K). Modular architecture was chosen to ease implementation at the expense of some additional computational overhead during execution. Each module retains its original data management and computational flow logic. Transfer of information among modules is accomplished via standard interface data files, including some as defined by the Committee on Computer Code Coordination[20] and others newly defined for this work.

The interface module retrieves material mass and temperature data from the thermal/hydraulics model, transfers the data from the thermal/hydraulics spatial grid to the spatial kinetics grid, and prepares cross section data for the spatial kinetics module. Following the subsequent flux computation, the interface module transfers the newly-calculated power distribution to the thermal/hydraulics spatial grid where it is used to calculate new mass and temperature distributions, closing the computational cycle. At the initial, steady state condition, this computational cycle is repeated until convergence is obtained. In the transient, each computational cycle represents one time step, advancing the transient simulation time.

The coupling techniques employed here are an extension of the techniques used successfully in prior analyses[21,22] of thermal reactor systems. Their implementation here was verified by testing that included numerical checks of mass and energy conservation, comparison of neutronics eigenvalue calculation results to stand-alone methods, and steady null-transient performance.

2.5 EXTENSIONS OF SAS4A/SASSYS-1 FOR HEAVY LIQUID METAL COOLANTS

The SAS4A and SASSYS-1 computer codes contain programmed correlations for coolant thermophysical properties, heat transfer correlations, and fluid dynamics pressure drop correlations. For this work, the experimental database on such information for lead (Pb) and lead-bismuth eutectic (Pb-Bi) was evaluated. The best available data was employed in a numerical fit to the correlations forms programmed in SAS4A and SASSYS-1. The new correlations were verified by comparisons to the original experimental basis, demonstrating that all fitting errors are well within the original experimental uncertainties. With these new properties and correlations, all of the SAS4A and SASSYS-1 single phase coolant heat transfer and coolant dynamics models are appropriate and accurate in heavy liquid metal applications.

3. APPLICATIONS MODEL AND INPUT DATA

3.1 MINOR ACTINIDE BURNER DESIGN

Example problem geometry and material compositions were taken from a recent OECD/NEA benchmark specification for an accelerator-driven, minor actinide burner design[23]. The benchmark serves as a computational reference for evaluation of calculational methods for systems used for transmutation of spent light water reactor fuel. The benchmark design was based on the Advanced Liquid Metal Reactor (ALMR) design, which in its original concept was a 471 MWt sodium-cooled, metallic-fueled fast reactor. For the benchmark exercise, the design was converted to a subcritical assembly driven by a proton accelerator producing neutrons by spallation in a centrally-located, liquid lead-bismuth (Pb-Bi) target. The sodium coolant was replaced with liquid Pb-Bi, and the fuel material was replaced with zirconium containing minor actinides and plutonium in the form of mononitrides. The original ALMR hexagonal subassembly design was retained, with a pitch of 0.1596 m (6.282 in.). The number of fuel pins in each subassembly was reduced from 271 to 217 to increase the coolant volume fraction and reduce the heavy liquid metal coolant pumping power requirement. In the benchmark specification, the initial reactor power was estimated to be 377 MWt based solely on the reduction in the number of fuel pins, and the corresponding neutron source in the target region was specified.

For this work, the two-dimensional r/z geometry specified in the benchmark was converted to three-dimensional hexagonal-z geometry, assuming the original ALMR subassembly pitch, hexcan dimensions, and cladding diameter and thickness. In the three-dimensional model, the r/z geometry fueled region volume was matched as closely as possible (difference less than 0.8%) by adjusting the number of subassemblies, and the benchmark fuel material masses were matched exactly by a corresponding adjustment of the isotopic densities. A plan view (1/6-core sector) of the resulting reactor design is shown in Fig. 1, which indicates the central target region, the fueled region, and the reflector region. In all the calculations reported here, liquid coolant was assumed to fill the entire axial extent of the target region, in contrast to the voided upper axial reflector region specified in the benchmark, in order to permit application of diffusion theory. A single thermal/hydraulic (pin) channel was used to represent all the pins in each unique fueled subassembly as shown in Fig. 1, yielding a 1/12 core symmetry in the spatial kinetics model. The subassembly numbering scheme in Fig. 1 is shown for future reference in the presentation of results.

3.2 GROUP CONSTANTS AND NEUTRON SOURCE GENERATION

For the kinetics analysis, region-dependent 9-group cross sections were generated based on ENDF/B-VI data. Using the MC2-2 code[24], homogeneous ultra-fine-group flux calculations were performed for individual materials of given nuclide densities and temperatures. The consistent P1 method was used with a group-independent buckling search for the fundamental mode spectrum calculations performed with 2082 groups. From these ultra-fine-group MC2-2 calculations, 230-group cross sections were determined for individual materials of given nuclide densities and temperatures. Using these 230-group material-dependent cross sections, region-dependent 9-group isotopic cross sections were generated from the 230-group full-core TWODANT[25] calculations. In this 9-group cross section generation, the fuel was divided into three radial regions and the reflector was divided into top, bottom, and radial reflectors. The target was treated as a single region.

In the benchmark specification, the external spallation neutron source produced with the NMTC code for a 1 GeV proton beam was provided. This spallation source was provided in terms of the spatial distribution and the spectrum given in fine group structure. In this study, the external source distribution was produced by collapsing the fine-group spectrum into nine groups and by converting the spatial distribution given in r-z geometry to one in hexagonal-z geometry. Finally, the source intensity was scaled such that the total power of a selected case was 377 MWt.

4. APPLICATIONS RESULTS

4.1 INITIAL STEADY STATE

For the application reported here, nodal diffusion theory results were obtained with DIF3D-K, and nodal P1 and P3 transport theory results were obtained with VARIANT-K. Integral results from eigenvalue (i.e. without source) and fixed source calculations at the steady state are given in Table I. All fixed source results were obtained using the same scaled source. Steady state powers for the eigenvalue calculations were taken from the corresponding fixed source calculation. The results labeled "Cold" in Table I were obtained on the first of the steady state iterations, when the fuel temperature is taken to be the base cross section temperature (707C) and the coolant density is uniform at the value corresponding to the reactor inlet temperature. The results labeled "Hot" in Table I are the converged steady state results. Table I shows that the DIF3D-K converged steady state power is very close to the benchmark value of 377 MW, and the VARIANT-K P1 power is close to the DIF3D-K result. The VARIANT-K P3 power is about 3% higher than the diffusion theory and P1 powers. The VARIANT-K P3 k_{eff} is about 0.2% higher than the diffusion theory and P1 values.

The results presented in Table I show very close agreement between the nodal diffusion and the P1 and P3 nodal transport solutions. The diffusion and transport calculations used the same cross section data file containing transport-corrected cross sections and isotropic scattering data. These results show that for this minor actinide burner core configuration, the spatial transport effects are less pronounced than those observed in other fast reactor core designs. This trend is attributed to the large dimensions of the core and the core composition, which make the fractional core leakage smaller than in earlier designs. Additionally the current design also has no control-rod zones and a uniform fuel concentration, and therefore has a comparatively reduced number

7

of material interfaces, which in turn minimizes spatial transport effects. The application of transport-corrected cross sections and isotropic scattering data in the current calculations resulted from the temporary absence of a coupled code module to process higher scattering moments into a format that could be used in the VARIANT transport module, which is capable of explicit anisotropic scattering if appropriate data are supplied. The effect of the higher scattering moments on the difference between the nodal diffusion solution and the transport solution (using P3 flux approximation and linearly anisotropic scattering) was studied using ancillary standalone DIF3D and VARIANT calculations. The results from the study indicated that the differences between the calculations are similar to those reported above, provided appropriately-determined transport-corrected cross sections are employed in the diffusion calculation. It was found that the Bell-Hansen-Sandmeier[26] correction of the total cross section provides good accuracy for the current core configuration and energy group structure.

Subassembly powers (MW) at the converged steady state are shown in Fig. 2, and the subassembly linear powers (kW/m) at the midplane are shown in Fig. 3. These results indicate that the principal difference among the three calculations is the total power, and that the normalized distribution of subassembly powers (or midplane linear powers) is nearly the same for all three calculations. For example, the peak-to-average subassembly powers calculated from the data in Fig. 2 are 1.854, 1.859, and 1.843 for DIF3D-K, VARIANT-K P1, and VARIANT-K P3, giving a variation of less than 1% between the DIF3D-K and VARIANT-K P1 results on the one hand and the VARIANT-K P3 result on the other.

4.2 NEUTRON SOURCE TRANSIENT

The first transient considered here simulates the spatial kinetics impact of a short-term, temporary interruption of the neutron source, such as might be caused by a accelerator beam drop and recovery. The thermal, hydraulic, and structural impacts of such a transient have been analyzed and reported in reference 1. This transient was assumed to be driven by a one-second long reduction of the steady-state neutron source to zero, followed by recovery to full strength. Results from analyses of this transient are given in Figs. 4 and 5.

Figure 4 shows the calculated reactor power (MW) as computed by DIF3D-K, VARIANT-K P1, and VARIANT-K P3. The plot indicates the difference in the initial power among the three calculations, and the immediate drop in the power in response to beam loss at 1 s. In all calculations, the power drops to decay heat with the loss of the neutron source, and then returns to near full power once the neutron source is restored. The effect of delayed neutron precursors decay following the source drop, although small, is evident in the slight slope of the power traces after 1 second.

Figure 5 shows plots of the transient, normalized power ratio between the highest (subassembly 3 in Fig. 1) and lowest (subassembly 23 in Fig. 1) power subassemblies. This normalized power ratio, or tilt, is a measure of the spatial kinetics effects during the transient. The results in Fig. 5 indicate that the only discernable difference among the DIF3D-K and VARIANT-K transient power shapes is during the time when the prompt neutron source is absent, and local power depends on decay heating and fissions due to delayed neutrons. During this time, the DIF3D-K and VARIANT P1 tilts are identical, and only slightly different from the VARIANT P3 tilt.

8

4.3 COOLANT FLOW AND TEMPERATURE TRANSIENT

The second transient considered here simulates failure of the coolant pumps power supply without termination of the neutron source. In the ALMR reactor design, this transient would be called an unprotected loss-of-flow (ULOF) sequence, a very low probability double-fault accident. The original ALMR design featured electro-magnetic (EM) pumps, equipped with an auxiliary flow-coastdown systems to provide a smoothed transition to natural circulation coolant flow. For the analysis reported here, the effect of this auxiliary system have been neglected. Results from analysis of this transient are given in Figs. 6 and 7.

Figure 6 shows normalized total and decay power histories and normalized coolant flow results for the hottest (channel 1) and coldest (channel 13) subassemblies in Fig. 1. The plotted results are taken from the coupled DIF3D-K calculation, but the normalized VARIANT-K P1 and P3 results are indistinguishable on the scale shown. The results show that in the first few seconds, the coolant flow decays rapidly while the power remains nearly constant. This power-to-flow mismatch results in a rise of the coolant temperature, and subsequently the fuel temperature. The positive fuel temperature reactivity coefficient of this design yields a slight increase in the reactor power as the flow decay ceases with the establishment of natural circulation. In the transition to a new equilibrium state, the coolant flow in the hottest subassembly remains positive, but the coolant flow in the coldest subassembly stagnates and becomes slightly negative for a time as the parallel flow system self-regulates to an equal pressure drop.

Figure 7 gives transient plots of the peak fuel, cladding, and coolant temperatures in comparison to the reactor inlet and coolant boiling temperatures. The plotted results are taken from the coupled DIF3D-K calculation, but the VARIANT-K P1 and P3 temperatures are similar with temperature differences of only a few degrees Celsius compared to the results shown due to the differences in the initial subassembly powers given in Fig. 2. The results show that the transient coolant temperatures stay well below the boiling point, which is elevated above the normal boiling point due to the weight of the heavy liquid metal coolant above the core. The cladding in channel 1, the hottest subassembly, is predicted to melt at around 7 s, indicating that beyond this point, cladding (and fuel) would begin to relocate in the heavier, upward flowing coolant. The reactivity effect of this cladding motion is not accounted for in the current analysis, because the core disruption models in SAS4A do not permit treatment of molten cladding in liquid coolant. However, the stainless steel cladding is a neutron absorber in the fast spectrum, and its removal from the core would be a positive reactivity effect. On the other hand, removal of fuel from the core is a strongly negative reactivity effect, and would thus act to reduce the reactor power to a final, equilibrium level.

CONCLUSIONS

The VARIANT-K nodal transport theory and DIF3D-K nodal diffusion theory spatial kinetics codes have been coupled with the SAS4A/SASSYS-1 liquid metal coolant analysis codes. The coupled codes have been used to analyze neutron source and coolant flow transients in a computational benchmark design proposed for a minor actinide-burning, subcritical reactor cooled by heavy liquid metal (Pb-Bi eutectic), and driven by a proton accelerator. The analyses focused on the impact of neutron transport and spatial kinetics effects by comparing the DIF3D-K nodal diffusion theory results with VARIANT-K P1 and P3 nodal transport theory results. All

calculations assumed isotropic scattering with transport-corrected total cross sections.

The principal differences among the three computational methods was found to be in the steady-state reactor power, which varied by about 3%. The relatively good agreement among the three methods can be attributed to the size and configuration of the benchmark design, and to the effectiveness of the transport correction to the total cross section for this application.

The good agreement among the three methods was also evident in results from transient source analyses, in which spatial kinetics effects were observed to be highly correlated to the presence (or absence) of the neutron source. For the system analyzed, it appears that a single power shape could be used very effectively during the time when the source is present. When the source is absent, the decay heat power shape appears to provide adequate accuracy. These conclusions would likely not be relevant for a design with moveable control rods, or with multiple, independent neutron sources.

Results from analyses of a coolant flow transient did not indicate significant spatial kinetics or transient transport effects. However, the analyses did indicate the possibility of thermally-induced phenomena (e.g. cladding and fuel melting and relocation) which were not dynamically modeled but which could have significant transient reactivity and local neutronics effects. Depending on the reactivity trends (positive or negative) and magnitudes, these effects may require spatial kinetics and transport analysis methods.

REFERENCES

1. D. C. Wade and F. E. Dunn, "Thermal and Mechanical Impacts on Sub-Critical Reactor and Coolant System Components Coming From Beam Trips and Fluctuations," Second Workshop on Utilisation and Reliability of High Power Proton Accelerators, OECD Nuclear Energy Agency, Aix-en-Provence, France, November 22-24, 1999.

2. G. Palmiotti, E. E. Lewis, and C. B. Carrico, "VARIANT: VARIational Anisotropic Nodal Transport for Multidimensional Cartesian and Hexagonal Geometry Calculation," ANL-95/40, Argonnne National Laboratory, October, 1995.

3. C. B. Carrico, E. E. Lewis, and G. Palmiotti, "Three-Dimensional Variational Nodal Transport Methods for Cartesian, Triangular, and Hexagonal Criticality Calculations," Nucl. Sci. Eng., 111, pp. 168-179, 1992.

4. G. Palmiotti, D. B. Carrico, and E. E. Lewis, "Variational Nodal Transport Methods with Anisotropic Scattering," Nucl. Sci. Eng. **115**, pp. 233-243, 1993.

5. E. E. Lewis, C. B. Carrico, and G. Palmiotti, "Variational Nodal Formulation for the Spherical Harmonics Equations," Nucl. Sci. Eng., **122**, pp. 194-203, 1996.

6. E. E. Lewis and G. Palmiotti, "Simplified Spherical Harmonics in the Variational Nodal Method," Nucl. Sci. Eng., **126**, pp. 48-58, 1997.

7. K. L. Derstine, "DIF3D: A Code to Solve One-, Two-, and Three-Dimensional Finite Difference Diffusion Theory Problems," ANL-82-64, Argonne National Laboratory, April, 1984.

8. A. Rineiski and J. Y. Doriath, "Time-Dependent Neutron Transport With Variational Nodal Method," Proceedings of the Joint International Conference on Mathematical Methods and Supercomputing for Nuclear Applications, American Nuclear Society, Saratoga Springs, New York, October 5-9, Vol. 2, pp. 1661-1669, 1997.

9. A. F. Henry, "The Application of Reactor Kinetics to the Analysis of Experiments," Nucl. Sci. Eng., **3**, pp. 52-70, 1958.

10. K. O. Ott and D. A. Meneley, "Accuracy of the Quasistatic Treatment of Spatial Reactor Kinetics, Nucl. Sci. Eng., **36**, pp. 402-411, 1969.

11. T. Taiwo, R. Ragland, G. Palmiotti, P. J. Finck, "Development of a Three-Dimensional Transport Kinetics Capability for LWR-MOX Analyses, Trans. Am. Nucl. Soc., **79**, pp. 298-299, November, 1999.

12. T. A. Taiwo, "DIF3D-K: A Nodal Kinetics Code for Solving the Time-Dependent Diffusion Equation in Hexagonal-Z Geometry, ANL/NPR-92/17, Argonne National Laboratory, October, 1992.

13. R. D. Lawrence, "The DIF3D Nodal Neutronics Option for Two- and Three-Dimensional Diffusion Theory Calculations in Hexagonal Geometry," ANL-83-1, Argonne National Laboratory, March, 1983.

14. T. A. Taiwo and H. S. Khalil, "The DIF3D Nodal Kinetics Capability in Hexagonal-Z Geometry: Formulation and Preliminary Tests," Proceedings of the International Topical Meeting on Advances in Mathematics, Computations, and Reactor Physics, American Nuclear Society, Pittsburgh, Pennsylvania, April 28-May 2, Vol. 5, pp. 23.2 2-1 to 23.2 2-15, 1991.

15. T. A. Taiwo and H. S. Khalil, "An Improved Quasistatic Option for the DIF3D Nodal Kinetics Code," Proceedings of the Topical Meeting on Advances in Reactor Physics, American Nuclear Society, Charleston, South Carolina, March 8-11, Vol. 2, pp. 469-481, 1992.

16. T. A. Taiwo and H. S. Khalil, "DIF3D-K: A Nodal Kinetics Code for Solving the Time-Dependent Diffusion Equation," Proceedings of the International Conference on Mathematics and Computations, Reactor Physics, and Environmental Analyses, American Nuclear Society, Portland, Oregon, April 30-May 4, Vol. 2, pp. 1171-1173, 1995.

17. T. A. Taiwo, et al., "SAS-DIF3DK Spatial Kinetics Capability for Thermal Reactor Systems," Proceedings of the Joint International Conference on Mathematical Methods and Super-Computing for Nuclear Applications, American Nuclear Society, Saratoga Springs, New York, October 5-9, Vol. 2, pp. 1082-1096, 1997.

18. J. E. Cahalan, et al., "Advanced LMR Safety Analysis Capabilities in the SASSYS-1 and SAS4A Computer Codes," Proceedings of the International Topical Meeting on Advanced Reactors Safety, American Nuclear Society, Pittsburgh, Pennsylvania, April 17-21, Vol. 2, pp. 1038-1045, 1994.

19. J. E. Cahalan and T. Y. Wei, "Modeling Developments for the SAS4A and SASSYS Computer Codes," Proceedings of the 1990 International Fast Reactor Safety Meeting, American Nuclear Society, Snowbird, Utah, August 12-16, Vol. II, pp. 123-132, 1990.

20. R. D. O'Dell, "Standard Interface Files and Procedures for Reactor Physics Codes, Version IV," LA-6941-MS, Los Alamos Scientific Laboratory, September, 1977.

21. E. E. Morris, "Impact of Spatial Kinetics in Severe Accident Analysis for a Large HWR," Proceedings of the International Topical Meeting on Advanced Reactors Safety, American Nuclear Society, Pittsburgh, Pennsylvania, April 17-21, Vol. 1, pp. 290-297, 1994.

22. H. S. Khalil, et al., "Coupled Reactor Physics and Thermal-Hydraulics Computations with the SAS-DIF3DK Code," Proceedings of the Joint International Conference on Mathematical Methods and Super-Computing for Nuclear Applications, American Nuclear Society, Saratoga Springs, New York, October 5-9, Vol. 2, pp. 1063-1071, 1997.

23. B. C. Na, P. Wydler, and H. Takano, "OECD/NEA Comparison Calculations for an Accelerator-Driven Minor Actinide Burner: Analysis of Preliminary Results," Second Workshop on Utilisation and Reliability of High Power Proton Accelerators, OECD Nuclear Energy Agency, Aix-en-Provence, France, November 22-24, 1999.

24. H. Henryson II, B. J. Toppel, and C. G. Stenberg, "MC2-2: A Code to Calculate Fast Neutron Spectra and Multigroup Cross Sections," ANL-8144, Argonne National Laboratory, June, 1976.

25. R. E. Alcouffe, F. W. Brinkley, D. R. Marr, and R. D. O'Dell, "User's Guide for TWODANT: A Code Package for Two-Dimensional, Diffusion-Accelerated, Neutral-Particle Transport," LA-10049-M, Los Alamos National Laboratory, February, 1990.

26.   G. I. Bell, G. E. Hansen, and H. A. Sandmeier, "Multitable Treatments of Anisotropic Scattering in Sn Multigroup Transport Calculations," <u>Nucl. Sci. Eng.</u>, **28**, pp. 376-383, 1967.
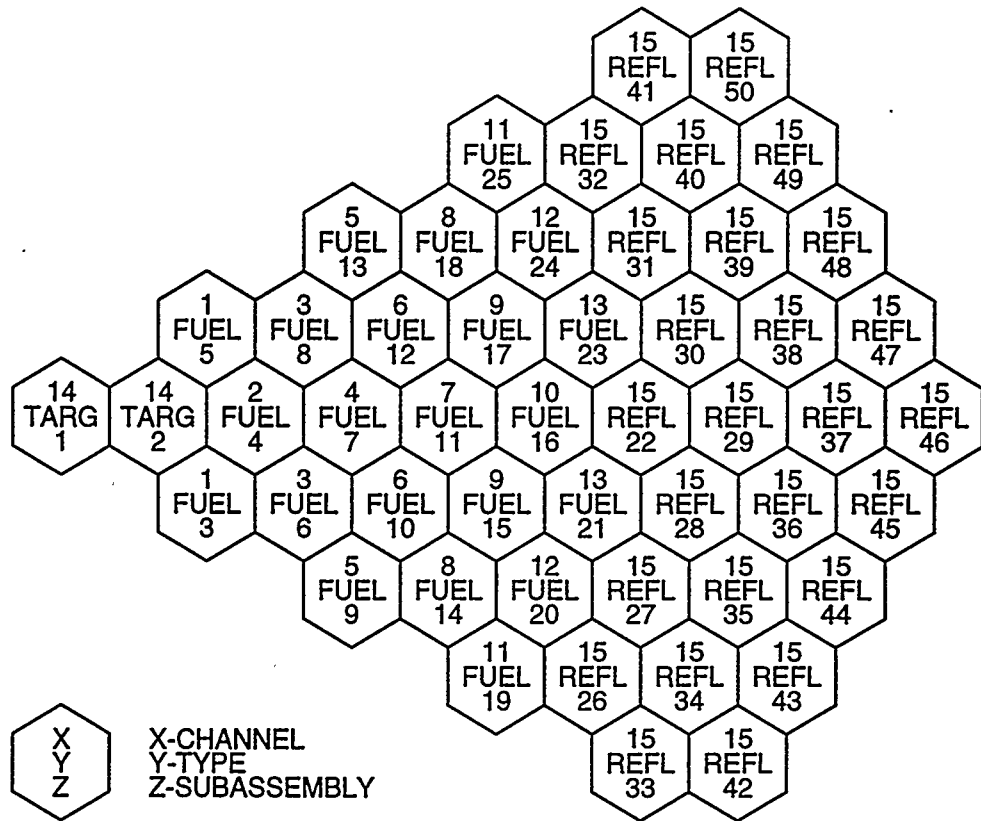
Fig. 1. Channel to Subassembly Assignment for Minor Actinide Burner Conceptual Design.
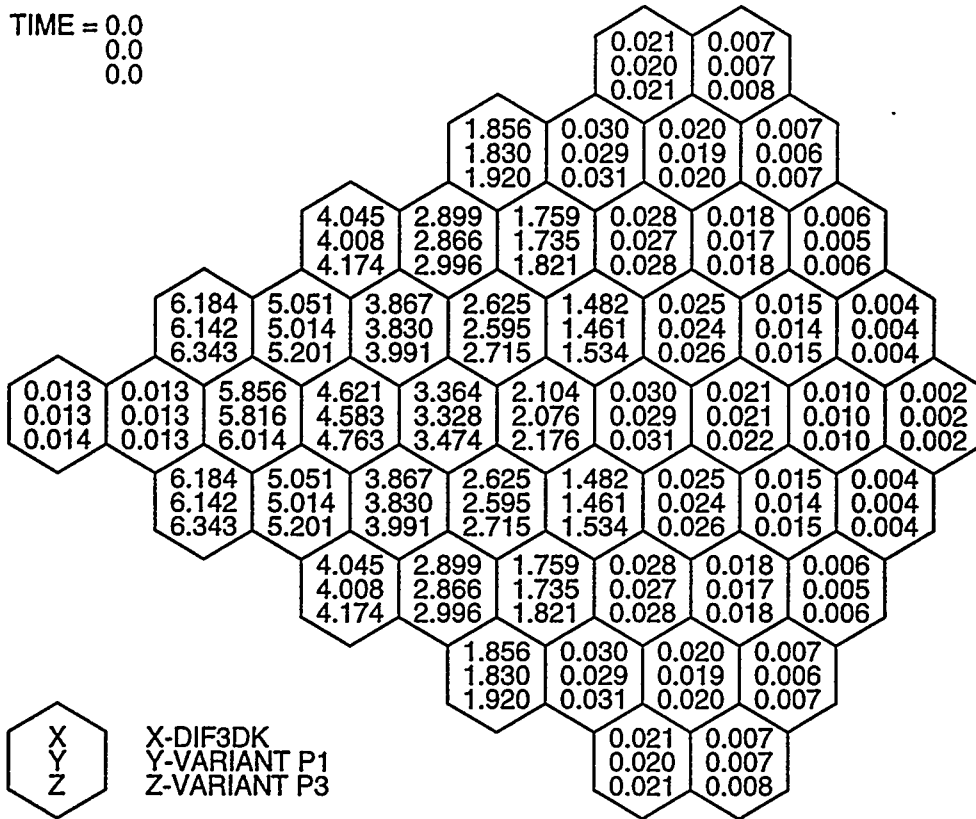
TIME = 0.0
       0.0
       0.0

							0.021	0.007	
							0.020	0.007	
							0.021	0.008	

						1.856	0.030	0.020	0.007
						1.830	0.029	0.019	0.006
						1.920	0.031	0.020	0.007

					4.045	2.899	1.759	0.028	0.018	0.006
					4.008	2.866	1.735	0.027	0.017	0.005
					4.174	2.996	1.821	0.028	0.018	0.006

			6.184	5.051	3.867	2.625	1.482	0.025	0.015	0.004
			6.142	5.014	3.830	2.595	1.461	0.024	0.014	0.004
			6.343	5.201	3.991	2.715	1.534	0.026	0.015	0.004

0.013	0.013	5.856	4.621	3.364	2.104	0.030	0.021	0.010	0.002
0.013	0.013	5.816	4.583	3.328	2.076	0.029	0.021	0.010	0.002
0.014	0.013	6.014	4.763	3.474	2.176	0.031	0.022	0.010	0.002

			6.184	5.051	3.867	2.625	1.482	0.025	0.015	0.004
			6.142	5.014	3.830	2.595	1.461	0.024	0.014	0.004
			6.343	5.201	3.991	2.715	1.534	0.026	0.015	0.004

					4.045	2.899	1.759	0.028	0.018	0.006
					4.008	2.866	1.735	0.027	0.017	0.005
					4.174	2.996	1.821	0.028	0.018	0.006

						1.856	0.030	0.020	0.007
						1.830	0.029	0.019	0.006
						1.920	0.031	0.020	0.007

							0.021	0.007	
							0.020	0.007	
							0.021	0.008	

X   X-DIF3DK
Y   Y-VARIANT P1
Z   Z-VARIANT P3

Fig. 2. Steady-State Subassembly Powers (MW) for Minor Actinide Burner Conceptual Design.

TIME = 0.0
        0.0
        0.0

					0.08 0.08 0.09	0.03 0.03 0.03

10.67 10.51 11.02 | 0.12 0.11 0.12 | 0.08 0.08 0.08 | 0.03 0.03 0.03

23.41 23.18 24.12 | 16.82 16.62 17.36 | 10.10 9.96 10.44 | 0.11 0.10 0.11 | 0.07 0.07 0.07 | 0.02 0.02 0.02

33.85 33.62 34.70 | 28.87 28.62 29.68 | 22.40 22.17 23.08 | 15.21 15.02 15.70 | 8.47 8.34 8.75 | 0.10 0.10 0.10 | 0.06 0.06 0.06 | 0.02 0.02 0.02

0.05 0.05 0.06 | 0.05 0.05 0.05 | 32.57 32.33 33.42 | 26.60 26.35 27.37 | 19.52 19.30 20.13 | 12.14 11.98 12.54 | 0.12 0.11 0.12 | 0.09 0.08 0.09 | 0.04 0.04 0.04 | 0.01 0.01 0.01

33.85 33.62 34.70 | 28.87 28.62 29.68 | 22.40 22.17 23.08 | 15.21 15.02 15.70 | 8.47 8.34 8.75 | 0.10 0.10 0.10 | 0.06 0.06 0.06 | 0.02 0.02 0.02

23.41 23.18 24.12 | 16.82 16.62 17.36 | 10.10 9.96 10.44 | 0.11 0.10 0.11 | 0.07 0.07 0.07 | 0.02 0.02 0.02

10.67 10.51 11.02 | 0.12 0.11 0.12 | 0.08 0.08 0.08 | 0.03 0.03 0.03

0.08 0.08 0.09 | 0.03 0.03 0.03

X
Y
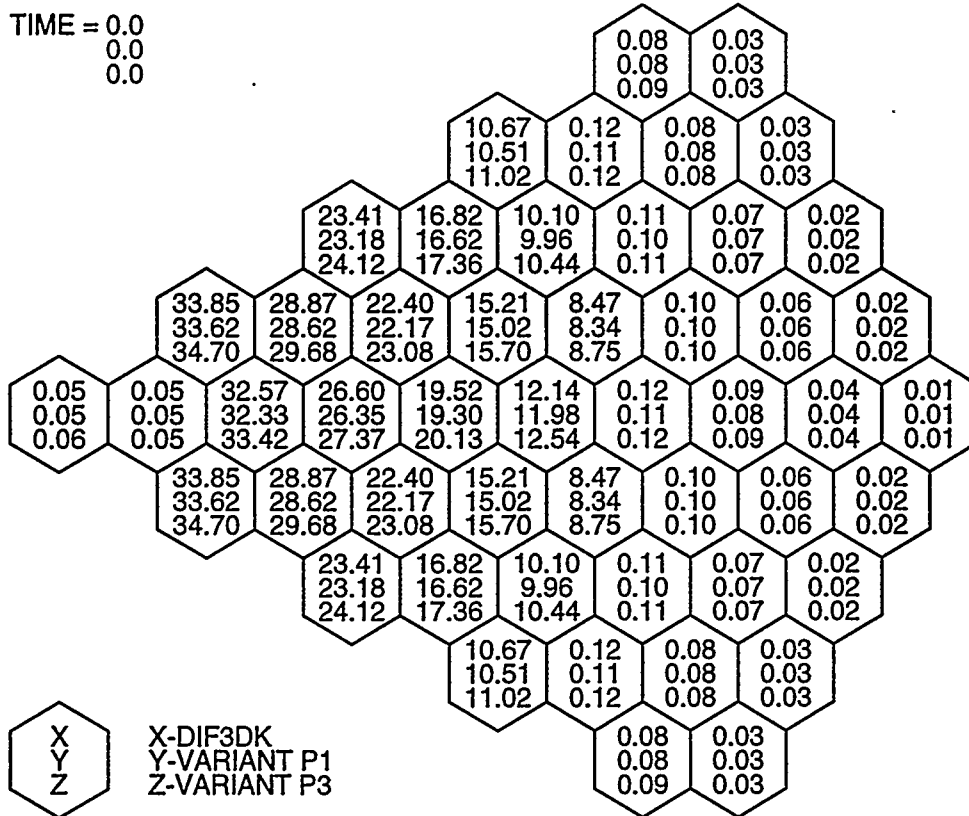Z

X-DIF3DK
Y-VARIANT P1
Z-VARIANT P3

Fig. 3. Steady-State Linear Powers (kW/m) for Minor Actinide Burner Conceptual Design.
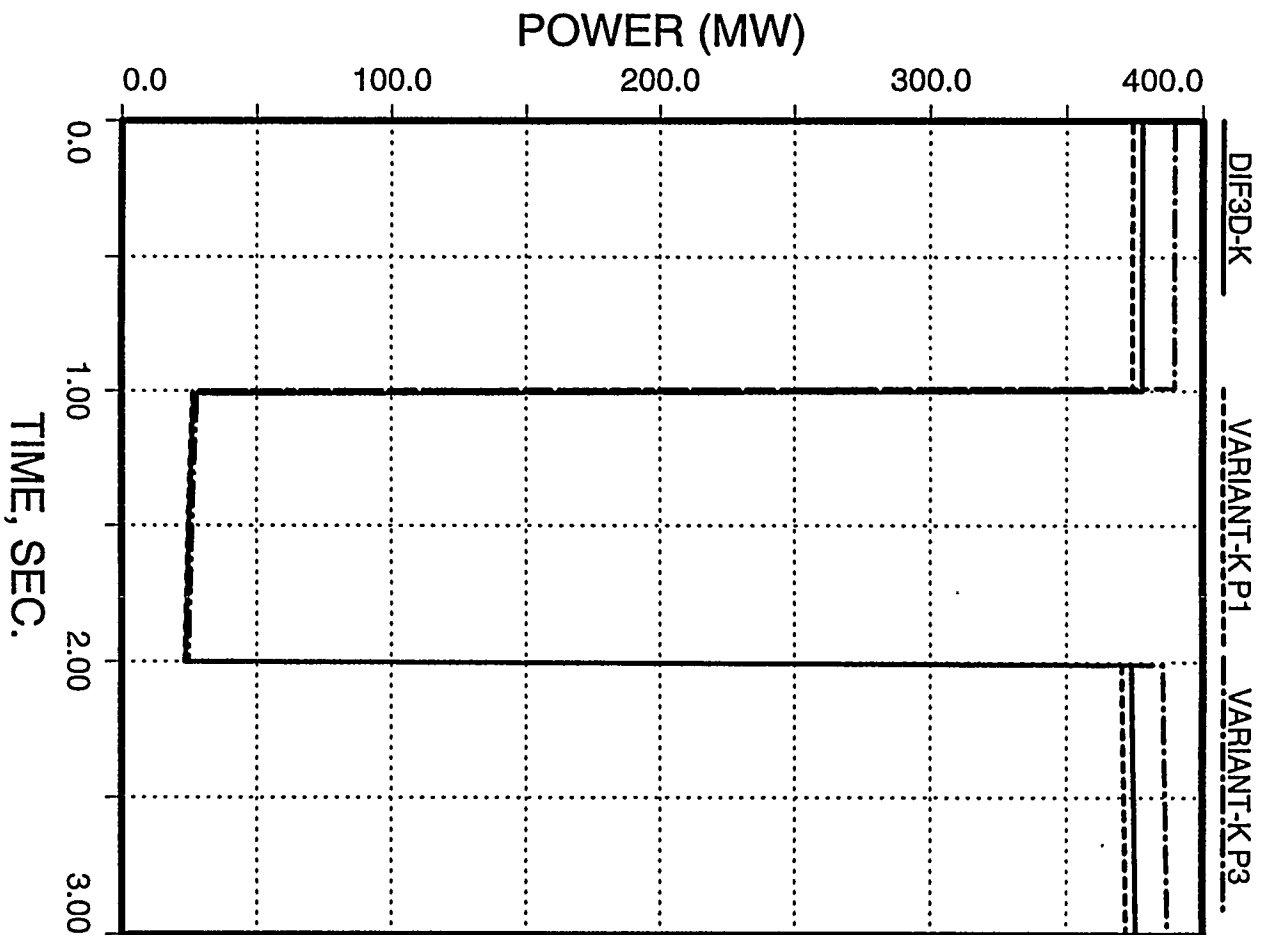
16

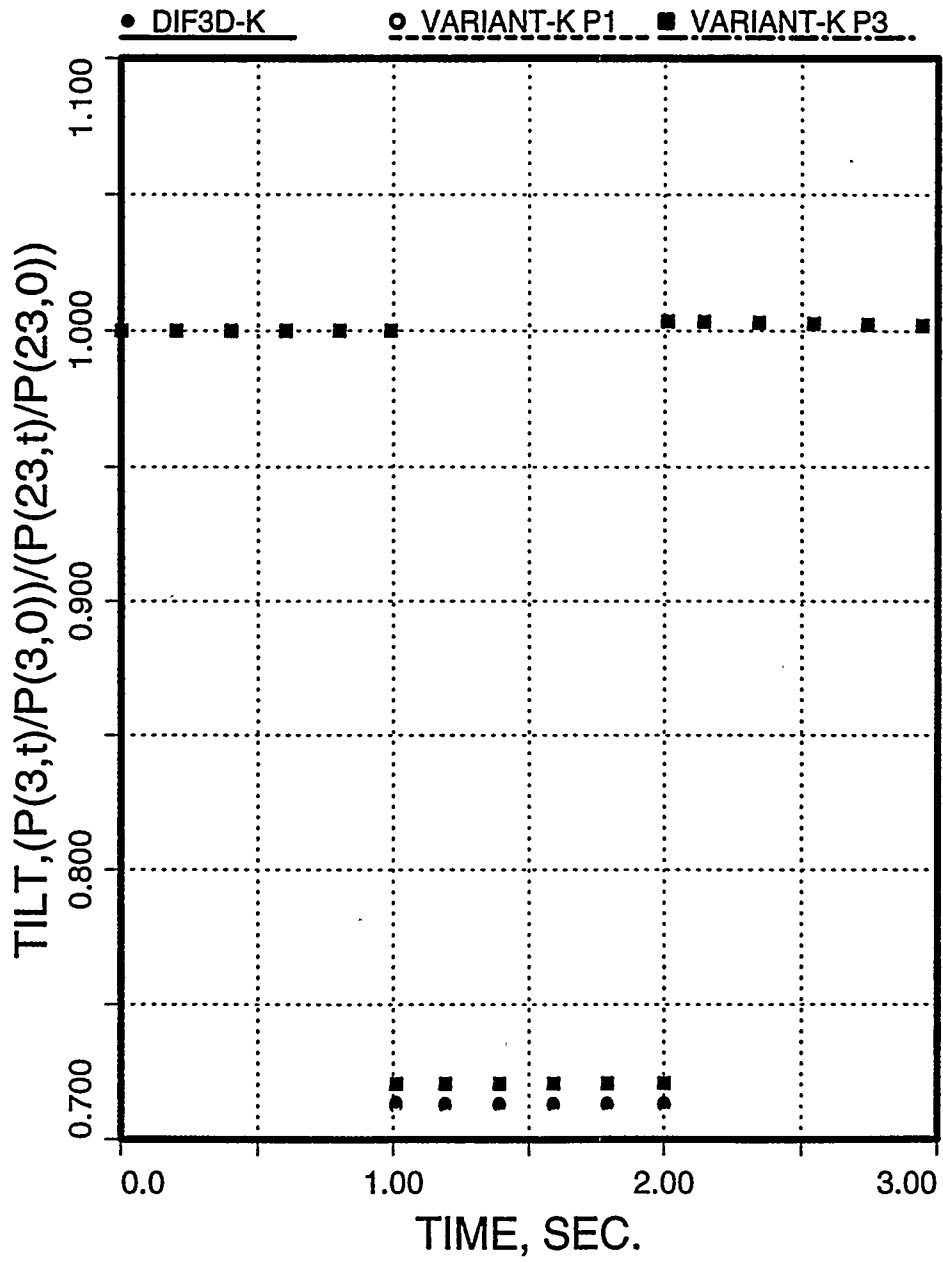Fig. 4. Power Histories for Source Transient.

17

Fig. 5. Subassembly Power Tilts for Source Transient.
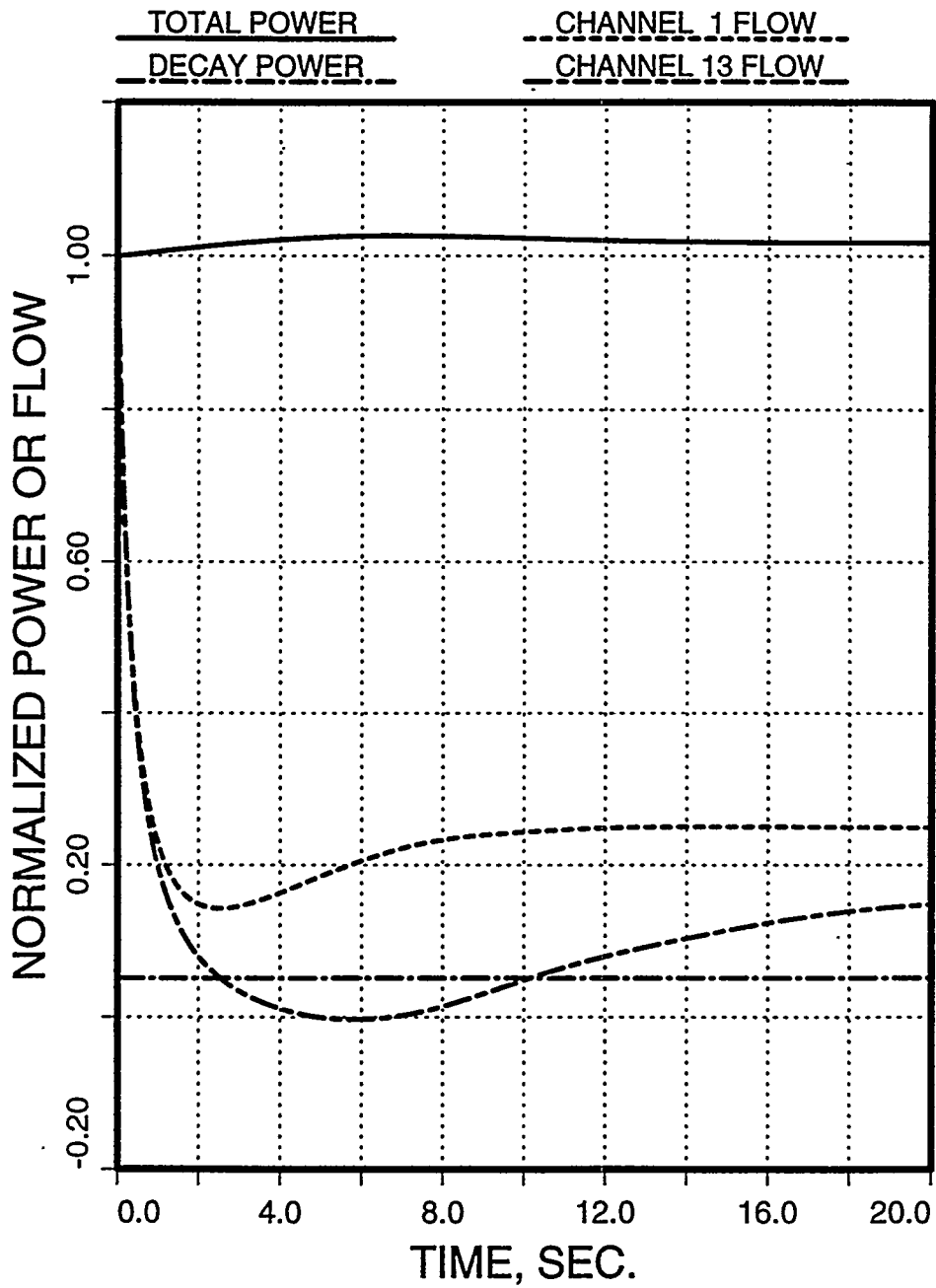
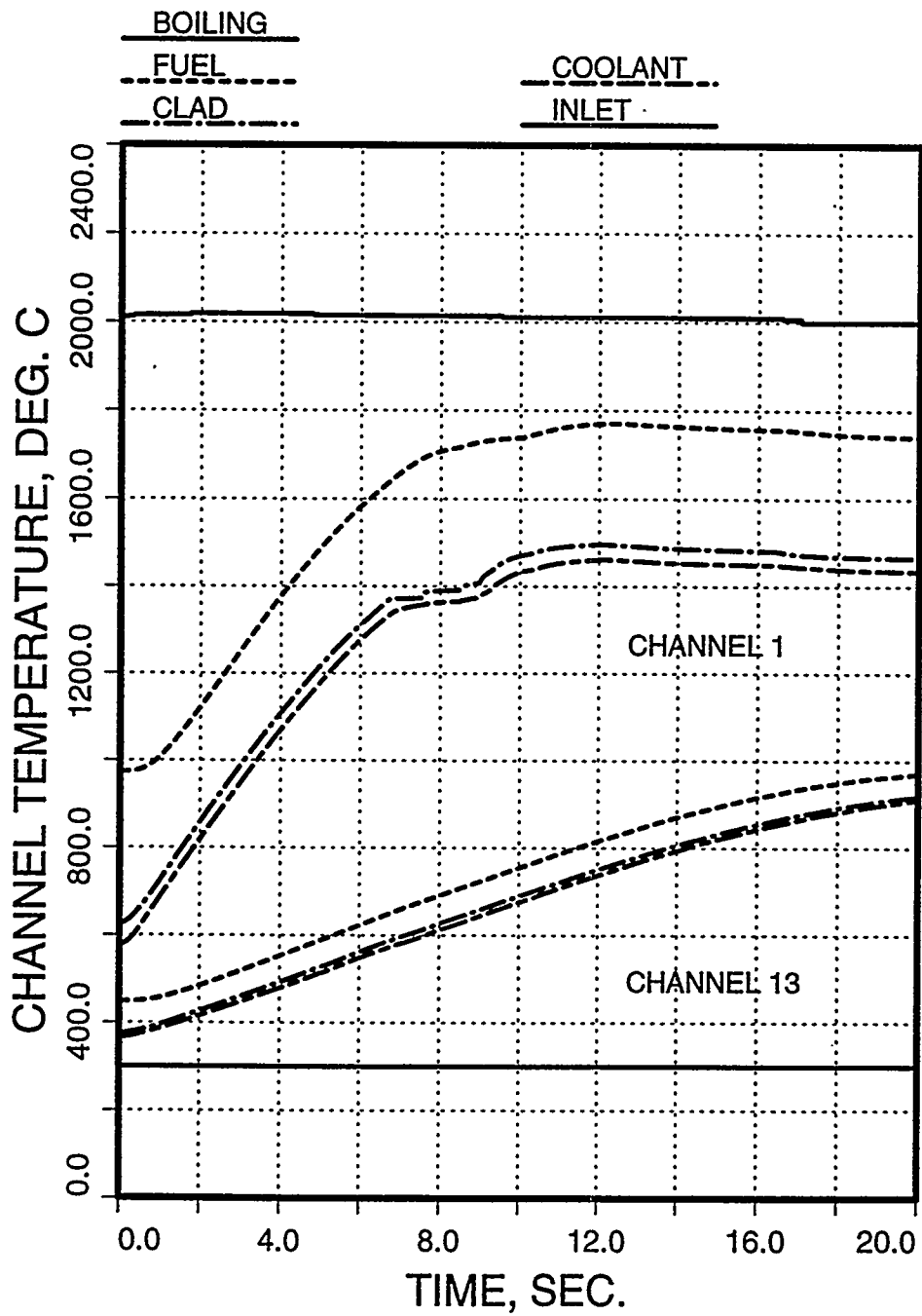Fig. 6. Normalized Power and Flow Histories for Coolant Flow Transient.

19

Fig. 7. Temperature Histories for Coolant Flow Transient.

Table I. Steady State Results.

	Total Power (MW) (Fixed source calculation)		k_{eff} (Eigenvalue calculation)	
	Cold[a]	Hot[b]	Cold[a]	Hot[b]
DIF3D-K	375.2	377.9	0.9557	0.9559
VARIANT-K P1	371.9	374.2	0.9551	0.9553
VARIANT-K P3	387.0	389.7	0.9574	0.9576

[a]Coolant density at inlet temperature and fuel cross sections at 707C.
[b]Coolant densities and fuel cross sections at operating conditions.